Science of the Total Environment 650 (2019) 1182–1194

Contents lists available at ScienceDirect

Science of the Total Environment

journal homepage: www.elsevier.com/locate/scitotenv

Physical, chemical, and toxicological characteristics of particulate emissions from current technology gasoline direct injection vehicles

Jiacheng Yang [a,b], Patrick Roth [a,b], Christopher R. Ruehl [c], Martin M. Shafer [d,e], Dagmara S. Antkiewicz [e], Thomas D. Durbin [a,b], David Cocker [a,b], Akua Asa-Awuku [a,b], Georgios Karavalakis [a,b,*]

[a] University of California, Bourns College of Engineering, Center for Environmental Research and Technology (CE-CERT), 1084 Columbia Avenue, Riverside, CA 92507, USA
[b] Department of Chemical and Environmental Engineering, Bourns College of Engineering, University of California, Riverside, CA 92521, USA
[c] California Air Resources Board, Sacramento, CA 95814, USA
[d] Department of Civil and Environmental Engineering, University of Wisconsin-Madison, Madison, WI, USA
[e] Wisconsin State Laboratory of Hygiene, University of Wisconsin-Madison, Madison, WI, USA

HIGHLIGHTS

- Cold-start dominated the production of black carbon and particle number emissions.
- Elevated PM emissions during the hard accelerations of the test cycle
- Overall, GDI PM samples showed that acute exposure toxicity was low for ROS generation and inflammatory potential.
- Correlation of trace metals and oxidative potential suggests a role for insoluble particles in inducing oxidative stress.

GRAPHICAL ABSTRACT

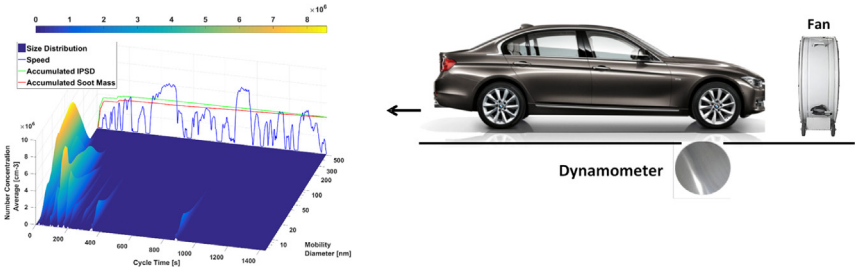

ARTICLE INFO

Article history:
Received 14 May 2018
Received in revised form 20 August 2018
Accepted 8 September 2018
Available online 10 September 2018

Editor: P. Kassomenos

Keywords:
Gasoline direct injection
PM emissions
Particle number
Toxicity
Oxidative stress

ABSTRACT

We assessed the physical, chemical and toxicological characteristics of particulate emissions from four light-duty gasoline direct injection vehicles when operated over the LA92 driving cycle. Our results showed that particle mass and number emissions increased markedly during accelerations. For three of the four vehicles tested, particulate matter (PM) mass and particle number emissions were markedly higher during cold-start and the first few accelerations following the cold-start period than during the hot running and hot-start segments of the LA92 cycle. For one vehicle (which had the highest emissions overall) the hot-start and cold-start PM emissions were similar. Black carbon emissions were also much higher during the cold-start conditions, indicating severe fuel wetting leading to slow evaporation and pool burning, and subsequent soot formation. Particle number concentrations and black carbon emissions showed large reductions during the urban and hot-start phases of the test cycle. The oxidative potential of PM was quantified with both a chemical and a biological assay, and the gene expression impacts of the PM in a macrophage model with PCR (polymerase chain reaction) and ELISA (enzyme-linked immunosorbent assay) analyses. Inter- and intra-vehicle variability in oxidative potential per milligram of PM emitted was relatively low for both oxidative assays, suggesting that real-world emissions and exposure can be estimated with distance-normalized emission factors. The PCR response from signaling markers for oxidative stress (e.g., NOX1) was greater than from inflammatory, AhR (aryl hydrocarbon receptor), or MAPK (mitogen-activated protein kinase) signaling. Protein production associated with inflammation (tumor necrosis factor alpha-TNFα) and oxidative stress (HMOX-1) were quantified and displayed relatively

* Corresponding author at: University of California, Bourns College of Engineering, Center for Environmental Research and Technology (CE-CERT), 1084 Columbia Avenue, Riverside, CA 92507, USA.
E-mail address: gkaraval@cert.ucr.edu (G. Karavalakis).

https://doi.org/10.1016/j.scitotenv.2018.09.110

high inter-vehicle variability, suggesting that these pathways may be activated by different PM components. Correlation of trace metal concentrations and oxidative potential suggests a role for small, insoluble particles in inducing oxidative stress.

1. Introduction

Gasoline direct injection (GDI) vehicles are on the rise and are receiving increased attention by automotive manufacturers because of their improved fuel economy and hence lower greenhouse gas (GHG) emissions compared to their port-fuel injection (PFI) counterparts (Xu et al., 2011). GDI engines combined with turbocharging and lightweighting technologies are one of the very few viable engine platforms to meet the Corporate Average Fuel Economy (CAFE) standards that have specified fuel economy to exceed 55 miles/gal (4.2 L/100 km) in passenger cars by 2025. Though the fuel economy and GHG benefits from GDI engines are clear, several studies have reported higher particulate matter (PM) and particle number emissions compared to other engine technologies such as PFI engines and modern diesel vehicles equipped with diesel particle filters (Zinola et al., 2016; Sobotowski et al., 2015; Karavalakis et al., 2014). The higher particulate emissions from GDI engines are largely due to the presence of fuel-rich regimes (resulting from the insufficient preparation of air-fuel mixtures) where soot particles are formed. In addition, the direct contact of fuel onto cold piston and cylinder walls (fuel wetting) leads to flame quenching, resulting in incomplete combustion and volatile organic compound (VOC) emissions (Attar and Xu, 2016; Piock et al., 2011).

The elevated particulate emissions from GDI vehicles are especially concerning given the context of increasingly strict PM emissions regulations in both the United States (US) and the European Union (EU). These regulations have been driven by the large and growing body of science implicating PM in a broad range of human health impacts. In the US, where PM regulations are expressed in terms of filter-collected mass emitted per mile, California implemented their LEV III light-duty PM standard of 3 mg/mile (1.9 mg/km) for model year 2017 vehicles and a 1 mg/mile (0.6 mg/km) target for model year 2025 vehicles over the Federal Test Procedure (FTP). In the EU, where PM regulations are in-place for both mass and particle number, the proposed Euro 6c solid particle number (i.e., the number of particles with diameters >23 nm after heating to 300 °C) limit for spark-ignition engines is at 6.0×10^{11} particles/km with a PM mass limit of 4.5 mg/km over the New European Driving Cycle (NEDC).

The physiochemical and toxicological characteristics of the PM emissions are as, or more, relevant to potential human health impacts than the mass emission factors. However, toxicological impacts of PM emissions, especially from GDI engines, are poorly understood. Several studies have examined the nature of particulate emissions from GDI engines as a function of fuel type, fuel injection architecture, aftertreatment control, and engine operating parameters (Chen et al., 2012; Chan et al., 2014; Barrientos et al., 2016). Particles from GDI engines are generally formed from fuel and lubricant oil and are complex agglomerates of volatile and non-volatile substances, both organic and inorganic (sulfate, nitrate, metal species) in nature (Piock et al., 2011). Karavalakis and co-workers (2015a) documented that greater aromatic hydrocarbon content in gasoline resulted in higher PM mass, particle number, and black carbon emissions from a fleet of GDI and PFI vehicles. Pirjola et al. (2015) showed a clear effect of lubricant oil on particle emissions from a modern GDI vehicle. Badshah et al. (2016) reported that under cold-start conditions the large majority of the total exhaust particles from GDI vehicles were solid soot and only a small fraction were semi-volatile.

A number of studies have shown that exposure to primary PM emissions from mobile sources is linked directly to adverse health implications (Bisig et al., 2018; Tzamkiozis et al., 2010; Seagrave et al., 2002). Epidemiologic and toxicological studies have reported that elevated levels of PM are associated with cardiopulmonary mortality and morbidity (Araujo and Nel, 2009; Bates et al., 2015; Reed et al., 2008). The underlying mechanisms via which PM exposure contributes to adverse human health outcomes are the subject of intense study and our understanding is incrementally expanding. Increasing evidence suggests that transition metals present in PM (e.g., iron, manganese, vanadium), as well as certain organic species (e.g., quinones) generate reactive oxygen species (ROS) that may be involved in producing respiratory symptoms (Rohr and Wyzga, 2012; Diaz et al., 2012; Charrier and Anastasio, 2012). Diaz et al. (2012) showed that primary particles emitted from a gasoline vehicle might be able to cause a change in the breathing patterns of male Sprague Dawley rats. Lund et al. (2007) showed that inhalational exposure to gasoline engine emissions resulted in increased aortic mRNA (messenger ribonucleic acid) expression of several genes, including matrix metalloproteinase-3 (MMP-3), MMP-7, and MMP-9, tissue inhibitor of metalloproteinases-2, endothelin-1 and heme oxygenase-1 (HO-1) in $ApoE^{-/-}$ (Apolipoprotein E)mice (an animal model of atherosclerosis). The authors concluded that exposure to gasoline exhaust results in vascular remodeling, as well as increased expression of markers of oxidative stress, which may contribute to the progression of atherosclerosis. A recent study showed that exposure to GDI exhaust contributes to upregulation of genes related to the metabolism of polycyclic aromatic hydrocarbons (PAHs) and oxidative stress (Maikawa et al., 2016). There is significant body of evidence documenting that insoluble particulate matter can initiate inflammatory cascades in lung tissues with resulting morbidity, including carcinogenesis and endothelial dysfunction (Freire et al., 2013; Tamagawa et al., 2008).

The primary objectives of this study were to advance our understanding of the physical and chemical properties of particulate emissions from current technology GDI light-duty vehicles and provide a new primary assessment of the oxidative stress potential and inflammatory responses of the emitted PM. Dynamometer testing was conducted using model year 2015 and 2016 GDI passenger cars on California E10 gasoline fuel over the LA92 cycle. The physical, chemical, and toxicological properties of the particulate emissions are discussed in the context of the influences of the driving cycle and engine technology.

2. Experimental

2.1. Vehicles, driving cycle, and measurement protocols

Emissions from four 2015 and 2016 model year GDI passenger cars (as described in Table S1, in the Supplementary Material (SM)) were characterized in this study. They are referred to as GDI_1, GDI_2, GDI_3, and GDI_4 throughout this manuscript. All vehicles were equipped with wall-guided fuel injection systems, operated with overall stoichiometric air-fuel ratios, and had three-way catalysts (TWCs). The vehicles were certified to meet either the Federal Tier 2, Bin 2 emission standards or the California LEV-II, SULEV emission standards (for PM mass, both are 10 mg/mile).

Each vehicle was exercised over the LA92 test cycle (also known as the California Unified Cycle, or UC), which is a dynamometer driving schedule for light-duty vehicles developed by the California Air Resources Board (CARB). The LA92 consists of three phases (i.e., cold-start, urban, and hot-start phases) and has a similar three-bag structure to the FTP

cycle. The LA92 is characterized by higher speeds, higher accelerations, fewer stops per mile, and less idle time than the FTP. Testing included at least duplicate LA92s using a commercially available California E10 fuel. Emissions measurements were conducted in CE-CERT's Vehicle Emissions Research Laboratory (VERL), on a Burke E. Porter 48-in. single-roll electric dynamometer using a Pierburg Positive Displacement Pump-Constant Volume Sampling (PDP-CVS) system.

2.2. PM sampling and extraction protocols

Particulate matter was sampled from the CVS dilution system and collected onto 47-mm polytetrafluoroethylene (PTFE) filters, following the procedures in 40 CFR 1065. Cumulative PM samples were collected over each LA92 cycle with flow-weighting mass flow controllers. Sample and control filters were frozen until analyzed. Emissions measurements of total and solid particle numbers, black carbon, and particle size distributions were also made. The testing methods for the real-time particulate measurements are provided in the SM.

Filters were transported on ice to the University of Wisconsin, Madison, where they were extracted in ultra-pure MQ water and the unfiltered extracts (containing both insoluble and water-soluble species) subjected to a suite of chemical and toxicological analyses using the following protocols. This extraction protocol provides for quantitative recovery of both soluble and insoluble species from the collection substrate. This is the most robust approach for assessing the total potential health impacts of the collected PM – recognizing that both soluble and insoluble species (and their interactions) contribute to biological responses. Previous studies by this group of authors have shown PM extraction efficiencies in the range of 82% to 104% using this extraction protocol (Hamad et al., 2016). Portions of the PM extract suspensions were digested and analyzed for 43 elements using magnetic-sector inductively-coupled plasma mass spectrometry (SF-ICPMS). The reactive oxygen species (ROS), generated by the water extracts were quantified with both a chemical method that measures the consumption rate of dithiothreitol (DTT), and an in vitro method that measures PM-induced production of ROS via a fluorescent probe in a rat alveolar macrophage (NR8383) cell line. The membrane-permeable ROS probe (2′,7′-dichlorodihydrofluorescein diacetate (DCFH-DA)) is de-acetylated within the macrophage cell by ubiquitous cytoplasmic esterases, which allows ROS species to convert DCFH to its fluorescent form, DCF. The probe is sensitive to the full range of ROS species (e.g. oxygen and hydroxyl radicals, hydrogen peroxide and singlet oxygen) produced intra-cellularly in response to cellular stimulation by redox-active inorganic and organic species. The DTT assay, in contrast to the macrophage ROS assay, is a purely chemical method - redox-active chemicals in the PM oxidize added DTT to its disulfide form and the rate of DTT loss is equated to the oxidative activity of the PM. The electron transfer reactions involved in the DTT oxidation are similar in many respects to the oxidative burst initiated by superoxide formation in the mitochondria of cells. The technique is responsive to redox-active organic compounds (e.g. quinones) and to many redox-active metals; however, metals are significantly less efficient at oxidizing DTT compared to reactive quinones. Despite the enhanced sensitivity of the DTT method to quinones, the concentrations of metals in most systems far exceeds those of reactive organics, and therefore, like the macrophage ROS protocol, the DTT assay should be considered as sensitive to the broad range of ROS-active species present in engine PM, both soluble and insoluble.

Cells exposed to the PM sample extracts were also assessed for signs of overt cytotoxicity via two well-established approaches: (a) propidium iodide (PI; Invitrogen, ThermoFisher Scientific) nucleic acid staining using flow cytometry, (b) the MTT assay (Molecular Probes Vybrant MTT Cell Proliferation Assay Kit) using a 96-well plate format and the absorbance plate reader. In addition, the expression of 29 genes (Table S2) in NR8383 macrophages exposed for 4 h to GDI PM water extract suspensions was also determined using Qiagen's Custom Rat RT^2 Profiler™ PCR (polymerase chain reaction) Array. Finally, expression of two specific proteins: tumor necrosis factor alpha (TNFα) and heme oxygenase 1 (HMOX-1), produced by the NR8383 cells exposed for 6 h to the PM extracts, was quantified via ELISA (enzyme-linked immunosorbent assay) methods. Detailed description of the methods utilized for the analyses are provided in the SM.

3. Results and discussion

3.1. Particle size distributions

The transient nature of the particle size distributions for GDI_2 and GDI_4 vehicles are illustrated in Fig. 1 and Fig. 2, respectively. In the interest of brevity, the particle size distributions for only GDI_2 and GDI_4 are shown in the main body of this work, while the figures for GDI_1 and GDI_3 are provided in the SM. GDI_2 and GDI_4 vehicles were considered as representative of the testing campaign, whereas they showed the lowest and highest PM formation, respectively. Fig. 1a shows the particle size distribution for the cold-start and hot-running phases (phases 1 and 2), while Fig. 1b shows the hot-start emissions (phase 3) for the GDI_2 vehicle. The cold-start phase dominated the overall particle size distribution, with the formation of particles occurring during the first 200 s. The particle peaks were centered in the nucleation mode at about 25 nm and the accumulation mode at about 60 nm in diameter. Overall, cold-start and hot-running particle size distributions were bimodal in nature, with higher proportions of accumulation mode particles at the cold-start and more nucleation mode particles present as the engine warmed up. Accumulation mode particles from GDI engines consist of carbonaceous chain agglomerates similar to those found in diesel engines (Badshah et al., 2016). The much higher concentrations of accumulation mode particles during cold-start could be related to poor fuel vaporization because of the lower combustion temperatures and pressures that can lead to very rich localized pockets of mixture and rapid formation and growth of soot particles (Cheng et al., 2001; Sakai et al., 2013). These observations are in agreement with other studies and a building consensus that the direct injection of fuel into the combustion chamber and the cold piston crown can lead to relatively slow evaporation and pool fires, contributing to the formation of soot (Badshah et al., 2016; Koczak et al., 2016; Peckham et al., 2011).

After the cold-start period, in the warmed-up engine, the particle populations have significantly decreased in modal size, with nucleation mode particles centered at 10 nm dominating the particle size distribution profile, as shown in Fig. 1a. It is reasonable to assume that the population of accumulation mode particles dropped due to the warming of engine and exhaust surfaces, as well as the less rich fuel-air mixture and the improved fuel vaporization. After the first 200 s, both the nucleation and accumulation mode particles were virtually eliminated, suggesting that the warmed-up engine lessens fuel wetting and its effect on global and local air-fuel ratios. The disappearance of the nucleation mode particles suggests that the TWC achieved its light-off temperature and significantly reduced the hydrocarbon and semi-volatile species that contribute to the formation of nucleation mode particles via condensation.

The third phase of the LA92 is much shorter than the first two phases (Fig. 1b). Analogous to the first two phases, particle size distributions were bimodal in nature; with higher levels of accumulation mode particles at the beginning of the hot-start followed by higher concentrations of nucleation mode particles. The nucleation mode was prominent during the majority of the hot-start phase. The large nucleation mode particle spikes were observed during accelerations as transients disrupt the control of global air-fuel ratios and exacerbate the heterogeneity of the cylinder charge (Sobotowski et al., 2015; Tan et al., 2014). It has been previously hypothesized that the origin of nucleation mode particles stems primarily from volatile hydrocarbons derived from unburned fuel and metallic particles contributed from the lubricant oil additive package (Pirjola et al., 2015). By the end of phase 3 the particles were

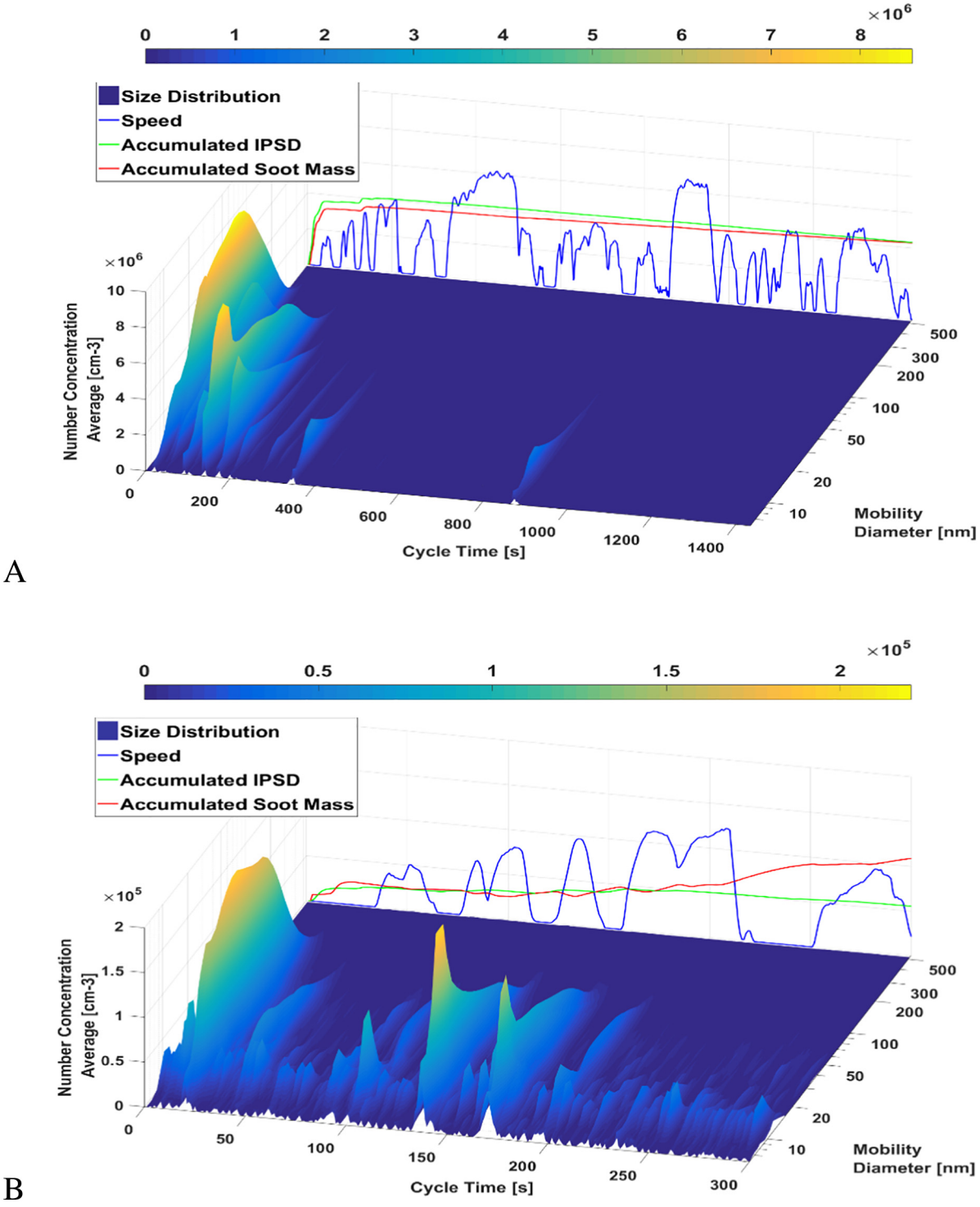

Fig. 1. (a–b): Particle size distributions for GDI_2 for phases 1 and 2 (top panel, A) and phase 3 (bottom panel, B) of the LA92 cycle. The drive trace is included for visual reference, as well as the cumulative soot mass IPSD mass emissions. Note the factor of ten difference between the vertical scales of the top and bottom panels.

very small in size with the mode at about 10–15 nm. It should be noted that for phases 1 and 2, peak concentrations were on the order of 10^6 cm^{-3}, whereas an order of magnitude reduction was observed after the hot-soak.

The particle size distribution profile for GDI_4 was different from GDI_2, as shown in Fig. 2 (a-b). For both the cold-start and hot-running phases, particle size distributions were dominated by accumulation mode particles, with a much smaller mode in the nucleation regime. After 600 s, the populations of accumulation mode particles decreased due to the warming of the engine. A significant spike in the accumulation mode was seen during the steep accelerations of the second phase. It is plausible that some fuel films survived the higher combustion temperatures associated with accelerations, causing pool fires and fuel pyrolysis, and consequently enhancing soot formation. Similar to GDI_2, phase 3 showed an order of magnitude reduction of accumulation mode particles (Fig. 2b). The distribution profile was decidedly unimodal, with a significant peak in the accumulation mode between 50 nm to 100 nm during the major hard accelerations of phase 3.

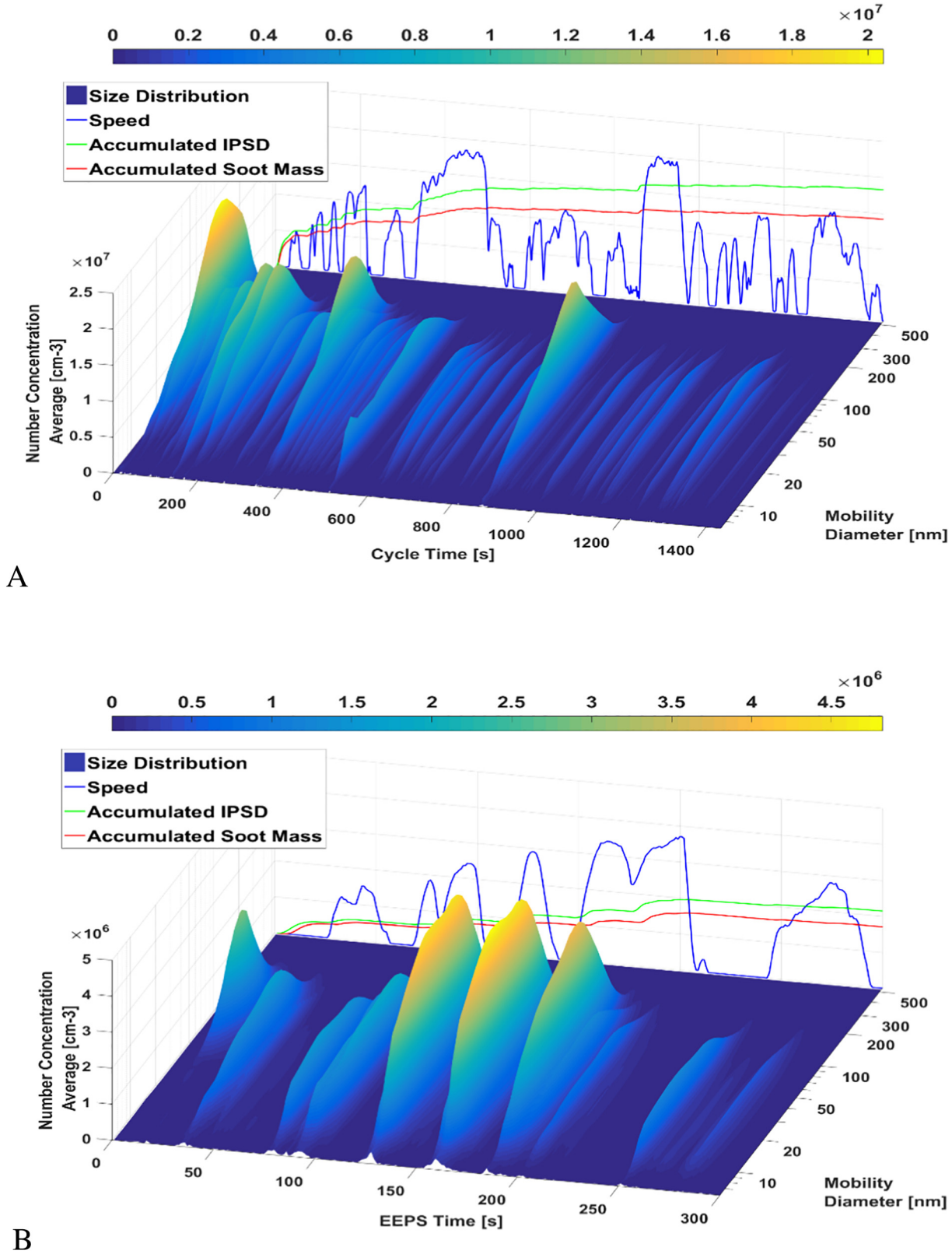

Fig. 2. (a–b): Particle size distributions for GDI_4 for phases 1 and 2 (top panel, A) and phase 3 (bottom panel, B) of the LA92 cycle. The drive trace is included for visual reference, as well as the cumulative soot mass IPSD mass emissions. Note the factor of ten difference between the vertical scales of the top and bottom panels.

The particle size distributions for GDI_1 and GDI_3 vehicles are shown in Figs. S1 and S2, respectively, in the SM. GDI_1 vehicle particle concentrations were overall lower than those of the GDI_4 vehicle, with higher particle concentrations in the nucleation mode at the start of ignition. This could be ascribed to the TWC being below its light-off temperature, allowing hydrocarbons from unburned fuel and other semi-volatile compounds to form nucleation mode particles. As the engine warmed-up, particle concentrations were considerably reduced, with

the particle size distribution profile being predominantly in the accumulation mode. Similarly, the phase 3 particle size distributions were dominated by accumulation mode particles, and the nucleation mode was practically absent. It can be assumed that the large surface area of the accumulation mode particles would favor the condensation of gas phase compounds onto pre-existing particles (heterogeneous nucleation) over new particles (homogeneous nucleation). Also, the TWC may have effectively removed semi-volatile gas-phase compounds, promoting evaporation of nucleation mode particles.

Particle size distributions for GDI_3 during phases 1 and 2 were dominated by nucleation mode particles, with the particle size distribution profile having a nearly unimodal distribution. Notably, large spikes in the nucleation regime were observed during the accelerations in phase 2. These phenomena were likely due to the higher exhaust gas temperature and the resulting enhanced formation of sulfuric acid with increasing engine load and engine speed, causing a stronger formation of nucleation mode particles (Herner et al., 2011). For the hot-start phase, the distribution was decidedly bimodal with the largest spikes being in the accumulation mode regime.

3.2. PM mass, black carbon, and particle number emissions

The gravimetric PM mass emissions are shown in Fig. 3, and they ranged from 0.26 to 4.72 mg/mile. While testing was performed over the LA92 cycle and not the certification FTP, PM mass levels were close to or below the 2017 PM mass emissions standards of 3 mg/mile. One of the vehicles (GDI_2) exhibited very low PM mass emissions compared to the other vehicles, even below the 2025 PM standards of 1 mg/mile. Previous studies conducted with older technology GDI vehicles equipped with wall-guided fuel injection systems over the FTP and LA92 cycles showed higher PM mass emissions than those reported here, ranging from 3 mg/mile to 8 mg/mile (Karavalakis et al., 2014; Zhang and McMahon, 2012). The low PM mass emissions from the GDI_2 vehicle is comparable to those reported in previous studies of older GDI vehicles with typically lower-emitting centrally-mounted injection systems, suggesting substantial progress in lowering PM mass emissions for some of the current technology GDI vehicles (Karavalakis et al., 2015b; Zhang and McMahon, 2012). These reductions in PM levels for the newer wall-guided GDI engines were likely a combination of improvements to the fuel injection system for controlling in-cylinder PM formation, such as increased fuel pressure, improved spray patterns, and reduced injector tip wetting.

Fig. 3 also shows the PM mass emissions calculated with the Integrated Particle Size Distribution (IPSD) method, which is an alternative for measuring PM mass at low emission levels (Quiros et al., 2015). This method evaluates real-time PM mass by integrating the products of the particle volume concentration derived from the particle size distribution and size-dependent particle effective density for each size/volume increment (Xue et al., 2016; Quiros et al., 2015). The results reported here were determined using the IPSD method with the EEPS Soot Matrix for each test vehicle. As observed in the gravimetric PM mass findings, the emission rates with the IPSD method varied across the test vehicles, ranging from 0.20 mg/mile to 5.30 mg/mile. For GDI_2 and GDI_3 vehicles, the IPSD method underestimates the gravimetric filter-collected PM mass by 23% and 11%, respectively, suggesting that particulates from these vehicles were mostly organic in nature and closely resembled the PM emissions characteristics of PFI vehicles (Sonntag et al., 2014). This is probably due to the fact that the EEPS soot matrix underestimated the nucleation mode concentration where most of the organic compounds are sourced from (Wang et al., 2016). For GDI_1 and GDI_4 vehicles, the IPSD method overestimates the PM mass by 12% and 18%, respectively. Though this agreement is quite reasonable considering method uncertainties, the overestimation suggests that the composition of particulate emissions from these vehicles was primarily elemental carbon (EC)/soot.

These hypotheses about the chemical nature of the PM are supported by the data on particle number emissions, as shown in Fig. 4, where for GDI_2 and GDI_3 vehicles EC/soot (solid particles) represented 41% and 35% of the particle number emissions respectively, leaving 59% and 65% that are either OC (non- or semi-volatile) or inorganic in nature (for GDI_1 and GDI_4, EC/soot represented 61% and 71% of the particle number emissions, respectively). This is also in agreement with the particle size distribution profiles for GDI_2 and GDI_3 vehicles, which were dominated by nucleation mode particles (Figs. 1 & S2), suggesting an abundance of semi-volatile species, which could potentially result in filter sampling artifacts from organics and semi-volatile species condensing onto filters and detected by gravimetric analysis, but not being accounted for by the IPSD method.

The black carbon emissions are shown in Fig. 3. Consistent with the PM mass emissions, GDI_2 showed the lowest black carbon emissions of the four vehicles tested. For all vehicles, black carbon was systematically lower than the gravimetric filter-collected PM mass, but accounted for a large fraction of that mass (91%, 45%, 77%, and 69% of the total PM mass for GDI_1, GDI_2, GDI_3, and GDI_4, respectively). Similar findings were

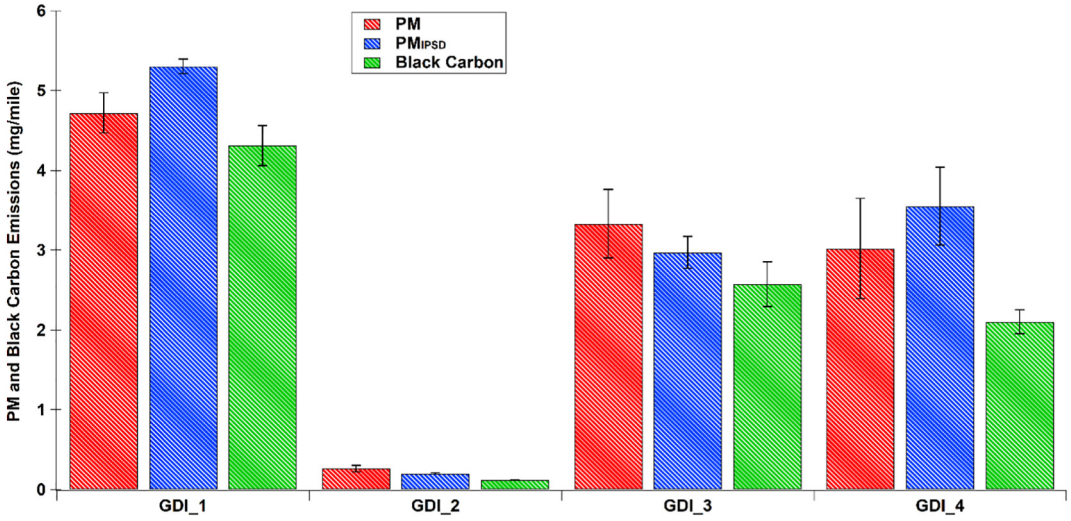

Fig. 3. Gravimetric PM, PM derived from integrated particle size distribution method (PM_{IPSD}), and black carbon/soot emissions expressed in mg/mile over the LA92 cycle. Data presented as mean ± standard deviation, $N = 2$.

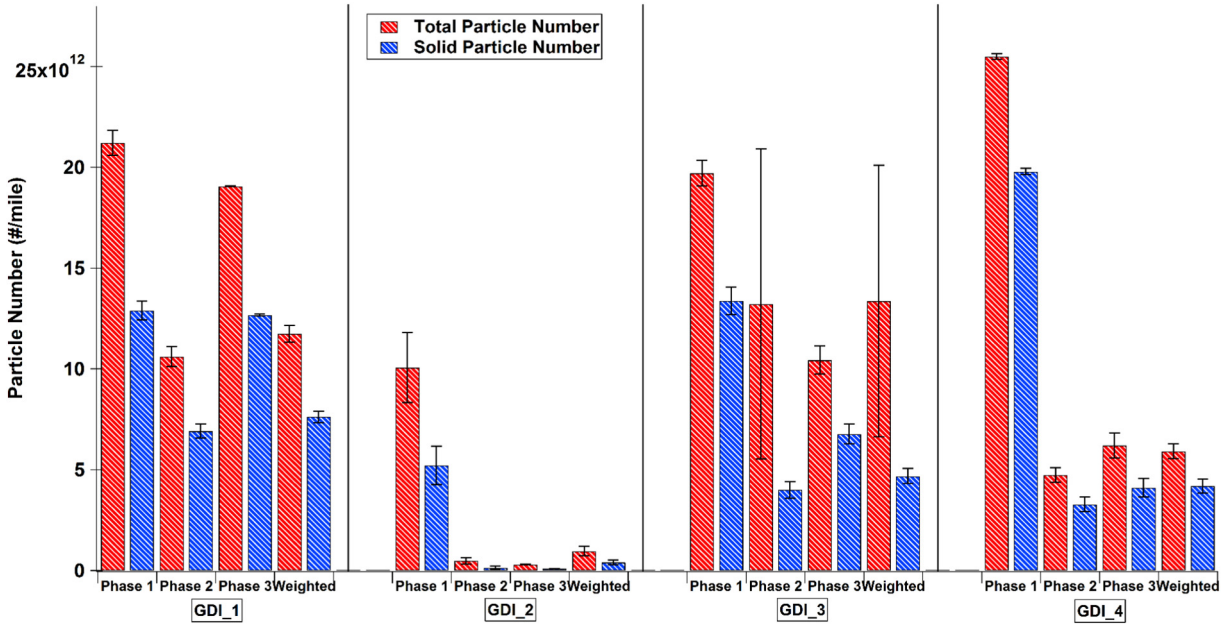

Fig. 4. Total and solid particle number emissions for all test vehicles for the cold-start (Phase 1), hot-running (Phase 2), hot-start (Phase 3), and the weighted LA92 cycle.

also seen in previous studies utilizing GDI vehicles (Karavalakis et al., 2014; Chan et al., 2014; Bahreini et al., 2015).

Fig. 4 shows the total particle number and solid particle number emissions for all test vehicles. Both total and solid particle number emissions showed consistent trends with PM mass. The cold-start phase of the LA92 had the highest particle emission factors, followed by the hot-start phase, and then the lowest emission factors during hot-running phase. The higher particle number emissions during the cold-start phase can be attributed to the reduced evaporation of the fuel wall film and the limited turbulent mixing with air, which cause a high amount of engine-out particulates (Piock et al., 2011; He et al., 2010). Several investigations have shown that in GDI engines, PM mass and number emissions are higher than those in PFI engines (Karavalakis et al., 2014; Bahreini et al., 2015). The increase in particulate emissions for GDI engines is likely due to the increased liquid fuel impingement on the combustion chamber walls that can result in liquid fuel that is not totally vaporized and well mixed at the start of combustion. This is turn may cause fuel pool fires generating higher PM emissions (Su et al., 2014; Szybist et al., 2011).

3.3. Oxidative potential

The oxidative potential of the PM emitted from the GDI vehicles was measured with both a biological (macrophage-mediated ROS production) and a chemical (dithiothreitol, or DTT oxidation) assay. Results are summarized on a per mile basis in Fig. 5a and on a per PM mass basis in Fig. 5b. On a per mile basis (Fig. 5a) the ROS data ranged over a factor of 70 and the DTT data by a factor of 20. However, inter- and intra- vehicle variability was substantially lower for both the ROS and DTT datasets when results were expressed on a per mass basis. An approximately 3-fold range was observed for the macrophage-mediated ROS and 2-fold range for the DTT data (Fig. 5b), implying a general similarity and consistency of the intrinsic (per mass basis) oxidative activity of PM emissions from these GDI technology vehicles. Moreover, when data for the low PM emitter vehicle (GDI_2) is excluded, the data ranges for the other 3 vehicles substantially overlap and little to no correlation is apparent between these two independent metrics of oxidative potential (DTT and macrophage-ROS) for either per mile or per PM mass normalization method. This likely reflects differences in the inherent sensitivity of the DTT and macrophage-ROS assay to the suite of organic and inorganic drivers of ROS. As mentioned above, one of the four vehicles (GDI_2) exhibited significantly lower oxidative potential in both ROS assays, particularly for the per mile metric, due to its substantially lower PM emissions. It is clear, therefore, that the wide range in per mile oxidative potential emissions is driven by this low PM emitting vehicle - if excluded, oxidative potential emission factors are remarkably consistent across vehicles.

The PM mass-normalized ROS outcomes from these 4 light-duty vehicles can be put into context by comparing to previously-published results using the same assay for both ambient PM samples and PM emitted from heavy-duty vehicles (Saffari et al., 2014a). The macrophage-mediated ROS induced by the PM emitted from vehicles in this study averaged 6409 μg ZU mg^{-1}, which is approximately mid-range of the values reported for a variety of urban ambient PM samples (Shafer et al., 2016), as well as for the ultrafine PM, the size range into which most vehicular emissions fall (Saffari et al., 2016; Daher et al., 2014). ROS ranged from 740 to 9200 μg ZU mg^{-1} in a large set of ambient urban European PM samples (Shafer et al., 2016), a slightly wider, but overlapping range to that of the tailpipe samples from the current study. This finding is consistent with the hypothesis that, in urban centers dominated by vehicular-sourced PM, vehicular emissions likely contribute a significant fraction of the ROS activity of urban ambient PM due to the presence of relatively non-labile, redox active species. In contrast, the DTT results of the current study, with an average of 56 nmol min^{-1} mg^{-1}, fall quite a bit higher than the reported activity of urban ambient PM from the above mentioned European study, which ranged from 5.2 to 20.0 nmol min^{-1} mg^{-1}. Thus, the mass-normalized, i.e. intrinsic DTT activity of PM from these vehicles was 2–10-fold higher than the typical urban ambient sample, possibly due to the higher organic content of GDI tailpipe emissions in comparison to ambient aerosols, though PM age and particle-size contrasts are also important factors. Previous studies have shown that a large portion of DTT activity can be due to the presence of reactive organic compounds such as quinones and humic like substances (Ghio et al., 2012). A study of quasi-ultrafine particles ($dp < 0.25$ μm) representing source, urban, rural receptor and desert locations across the Los Angeles air basin concluded that water soluble organic carbon (WSOC), water insoluble organic carbon (WIOC), EC, and hopanes had a combined contribution that explained up to 88% of the DTT activity (Saffari et al., 2014b). It should be pointed out that the current study's data range

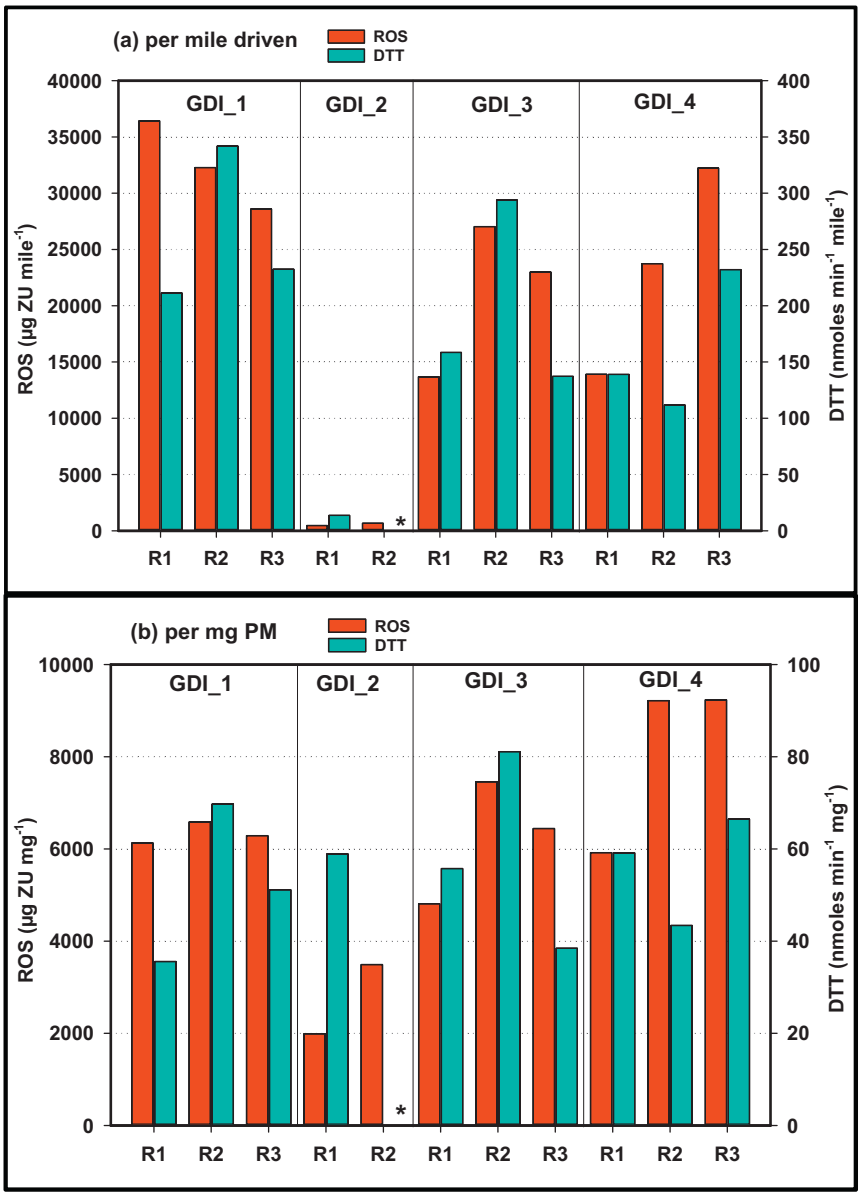

Fig. 5. Macrophage-based ROS and acellular DTT oxidation as two measures of oxidative potential of vehicular emissions. Data expressed on per mile basis (a) and per mg of PM mass (b), indicative of the intrinsic activity of the particles. R1–R3 represent replicate samples collected for the same vehicle. Note that the asterisk (*) in the plot indicates that the assay was not performed due to insufficient PM mass.

for the mass-normalized DTT falls well within the range of DTT activities determined in other quasi-ultrafine particle studies, including a summer study characterizing diurnal trends in urban PM from downtown Los Angeles. This study also found a high correlation between DTT and WSOC (Verma et al., 2009) suggesting that organic components of vehicular emissions are likely important drivers of their DTT activity. Therefore, as with the macrophage-ROS and metals, the current study's data is consistent with tailpipe emissions being a significant source, if not a dominant one, of DTT activity in urban ambient PM.

3.4. Water extractable metals

A total of 45 elements were characterized in the PM extracts, as shown in Table 1. Sulfur (S), which is sourced from both the fuel and lubricant oil (Pirjola et al., 2015) was the most abundant element, with an average emission factor of 29.9 μg/mile. The element with the second highest emission factor was iron (Fe) (averaging 12.4 μg/mile), followed by calcium (Ca), aluminum (Al), phosphorus (P), sodium (Na), potassium (K), and chromium (Cr) (averaging between 0.96 and 7.62 μg/mile). These elements can be emitted from several sources, including engine wear (abrasion from piston ring, cylinder liner, valves, etc.), combustion of fuel and lubricant oil, the lubricant oil additive package, and from tailpipe emission catalysts. Platinum-group element (PGE) emissions, primarily sourced from TWC, including those of platinum (Pt), palladium (Pd), and rhodium (Rh) were very low (averaging from 0.001 to 0.21 μg/mile). PGE emissions are released from the TWCs in PM form, primarily as the metal (oxidation state = 0) species, but oxides can represent a significant fraction (Hyde and Sankar, 2014; Moldovan, 2007).

Redox-active transition metals, such as vanadium (V), chromium (Cr), manganese (Mn), iron (Fe), nickel (Ni), and copper (Cu) were measured at relatively high concentrations in all vehicles, with their emission factor sum averaging from 5.2 μg/mile to 24.7 μg/mile (a range comparable to that of measured variation in ROS activity). Redox-active transition metals are known to facilitate the generation of ROS that can damage cellular membrane lipids, proteins or enzymes,

Table 1
Emission factors (in ng per mile) for PM elements detected by ICPMS, ranked by the sum of the averages for each of the four vehicles. Quoted uncertainty is the standard deviation. Also included are correlation coefficients with the ROS and DTT methods for measuring generation of reactive oxygen species and ELISA protein expression. Correlation coefficients of >0.5 are highlighted in bold.

	ng/mile				r^2			
	GDI_1	GDI_2	GDI_3	GDI_4	ROS	DTT	HMOX	TNF-α
S	56,000 ± 46,000	1570 ± 120	43,700 ± 21,600	18,500 ± 17,200	0.24	0.22	0.06	0.06
Fe	6800 ± 4400	4500 ± 1090	15,900 ± 11,100	22,400 ± 24,000	0.25	0.21	0.17	**0.51**
Ca	7210 ± 920	5660 ± 520	9410 ± 900	8200 ± 2260	0.19	0.18	0.03	0.13
Al	3550 ± 640	3400 ± 1660	2910 ± 800	6960 ± 4600	0.12	0.18	0.18	0.06
P	3570 ± 1200	1140 ± 50	3400 ± 580	3310 ± 1100	**0.59**	**0.61**	0	0.39
Na	2010 ± 550	1790 ± 0	2130 ± 170	2040 ± 1030	0.11	0.04	0.02	0.07
K	484 ± 106	1720 ± 43	1950 ± 940	809 ± 446	0.36	0.09	0.02	0.11
Zn	992 ± 137	387 ± 13	1670 ± 600	869 ± 535	0.33	0.41	0.01	**0.5**
Cr	1130 ± 931	339 ± 235	1420 ± 850	966 ± 731	**0.51**	0.4	0.01	0.41
Ti	891 ± 153	354 ± 22	848 ± 645	395 ± 172	0.24	**0.55**	0.18	0.39
Mg	744 ± 130	585 ± 158	578 ± 269	545 ± 252	0.15	0.46	0.1	0.49
Ni	441 ± 256	168 ± 119	667 ± 411	823 ± 716	0.39	0.32	0.1	**0.52**
Mo	627 ± 85	101 ± 26	571 ± 154	141 ± 75	0.41	0.43	**0.59**	0.14
Cu	162 ± 28	101 ± 6	359 ± 117	326 ± 212	0.24	0.2	0.12	0.39
Ce	259 ± 61	23 ± 2	297 ± 171	285 ± 235	**0.62**	**0.51**	0.01	**0.68**
Pd	123 ± 12	13 ± 2	395 ± 94	327 ± 193	0.26	0.16	0.17	0.29
Mn	96 ± 30	59 ± 21	227 ± 99	212 ± 214	0.23	0.24	0.08	0.48
Sr	254 ± 41	22 ± 9	26 ± 8	46 ± 20	0.44	0.32	0.44	0
Sn	87 ± 51	44 ± 1	129 ± 43	66 ± 2	0.16	0.28	0.01	0.22
La	91 ± 23	7 ± 4	40 ± 27	106 ± 85	**0.63**	0.4	0.03	0.35
Nd	41 ± 10	4 ± 1	43 ± 25	22 ± 20	**0.61**	**0.61**	0.15	0.49
W	12 ± 5	17 ± 3	30 ± 15	25 ± 20	0.04	0.14	0.12	**0.63**
Co	16 ± 8	15 ± 4	27 ± 12	15 ± 9	0.04	0.05	0.01	0.23
Li	16 ± 1	8 ± 6	9 ± 0	38 ± 10	0.22	0.08	0.47	0.01
Pb	17 ± 7	8 ± 5	21 ± 7	24 ± 11	0.14	0.08	0.13	0.04
Y	43 ± 10	2 ± 0	9 ± 2	5 ± 3	0.47	0.29	**0.54**	0
Pr	1 ± 0	1 ± 1	24 ± 11	26 ± 20	0.13	0.09	0.32	0.3
As	9 ± 1	5 ± 3	13 ± 7	15 ± 4	0.16	0.02	0.13	0.03
V	10 ± 6	4 ± 0	10 ± 3	9 ± 4	**0.54**	0.29	0.04	0.18
Ag	4 ± 1	3 ± 2	9 ± 8	10 ± 13	0.18	0.26	0.09	**0.62**
Sb	8 ± 5	2 ± 0	7 ± 2	5 ± 2	0.49	0.68	0.02	0.47
Rh	2 ± 0	0 ± 0	1 ± 1	8 ± 5	0.29	0.12	0.36	0.14
Rb	2 ± 1	3 ± 1	3 ± 1	3 ± 1	0	0.01	0.17	0.35

and DNA (Jomova et al., 2012), and importantly result in initiation of a pro-inflammatory cascade. The six redox-active transition metals listed above were weakly to moderately correlate with both the DTT and the ROS assay activities (r^2 of 0.25 to 0.46 for DTT and r^2 of 0.18 to 0.50 for ROS (Table 1). These results, though the sample number is small, contrast in-part to some previously reported chassis dynamometer data where both ROS and DTT assays showed good correlations with the redox-active transition metals (Karavalakis et al., 2017; Verma et al., 2010). Strong correlations were seen between the total sum of water-extractable metals and ROS (r^2 of 0.85) and DTT (r^2 of 0.92). Interestingly, molybdenum (Mo) was detected in relatively high levels compared to other metals (averaging at 0.36 μg/mile), with GDI_1 and GDI_3 having the highest emission concentrations, which were also the vehicles with the highest black carbon emissions. Mo-nanoparticles may be sourced from the additive package in the lubricating oil and have been reported to induce significant cytotoxicity and generate ROS (Siddiqui et al., 2015; Uy et al., 2014). Under the present test conditions, it is possible that Mo also played some role in the generation of ROS both in the DTT and macrophage-ROS assays.

Several rare earth elements (Ce, La, Nd), as well as Cr and Ti, exhibited moderate correlations with both ROS and DTT activity. The similar reactivity profiles of ROS and DTT lend support to the robustness of these correlations. These correlations may suggest a role for small insoluble particles in inducing oxidative stress, either directly, or by providing a catalytic particle surface.

3.5. Gene marker expression analysis

mRNA from the NR8383 macrophages exposed to the PM emitted by three of the four GDI vehicles (insufficient mass was available from the lowest-emitting vehicle – GDI_2) was analyzed for expression of 29 genes, including 2 housekeeping genes (Table S2). The genes selected for this study include those associated with oxidative stress and inflammatory signaling including asthma, as well as AhR (aryl hydrocarbon receptor) and MAPK (mitogen-activated protein kinase) signaling markers. Overall, the vehicular emission-induced gene expression changes (i.e., fold regulation relative to the untreated controls) were quite low (with only 3 genes exhibiting regulation over 2-fold change), likely due in-part to the relatively low masses of PM available for the macrophage exposures and the relatively short, single-dose, exposure duration (one time-point at 4 h). Collection of adequate PM mass from traditional chassis dynamometer is a serious problem in all toxicologically directed studies, particularly from modern low PM emitting vehicles. Though we extended collection periods as long as feasible and performed multiple experiments on a given vehicle, the mass available for chemical and toxicological characterization was typically <200 μg.

Of the gene categories listed above, the greatest regulation was observed within the oxidative stress signaling markers (Tables S3 & S4). The upregulation of NADPH (nicotinamide adenine dinucleotide phosphate) oxidase 1 (Nox1) expression in 2 out of 3 vehicles, as well as quite consistent downregulation (2- to 3-fold in 5 out of 9 samples) of myeloperoxidase (MPO), both of which play an important role in the respiratory burst signaling, confirm that the vehicular exhaust can lead to oxidative stress in macrophages (Hideki, 2008; Odobasic et al., 2016). The downregulation of MPO measured at 4 h exposure likely reflects regulatory feedback signaling initiated after the induction of ROS production (as measured at 2.5 h of exposure via the cellular ROS assay). The mRNA gene expression patterns in this very same exposure system can change within 1 h (Sijan et al., 2015). In addition, a small

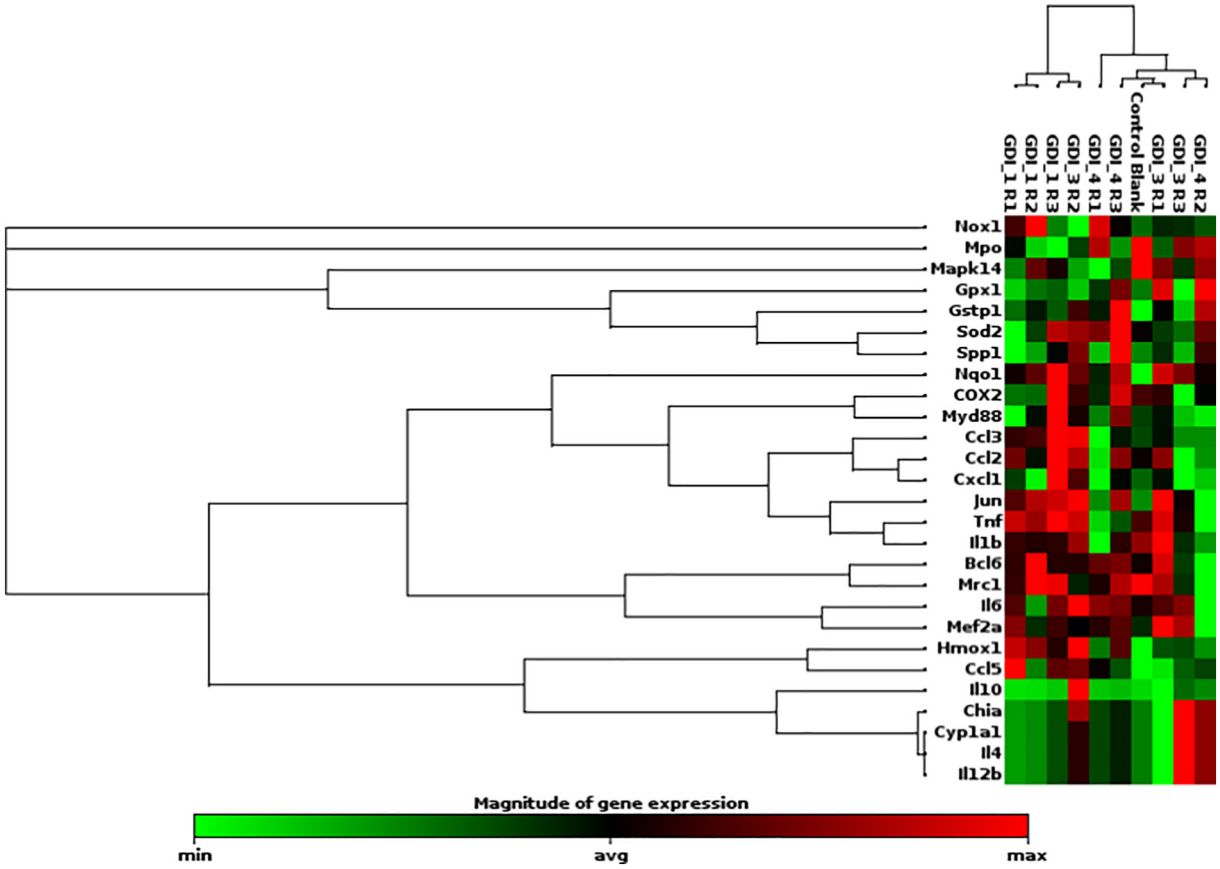

Fig. 6. Non-supervised hierarchical clustering of gene regulation (mRNA level fold change relative to untreated control) upon 4 h exposure to vehicular exhaust extracts of 3 vehicles. Dendrograms indicate co-regulated genes as well as similarities of gene expression patterns between individual samples.

upregulation of the anti-inflammatory cytokine IL-10 (Interleukin 10) was observed in our data set, which could also suggest activation of protective mechanisms in response to the aerosol exposure. While the overall fold regulation range for a given marker in the current study was quite small, the gene expression data can be used to look for signaling patterns and/or sample relationships using tools like hierarchical clustering. Fig. 6 presents such an analysis of the gene expression data. Replicate samples from the GDI_1 exhibit a very similar pattern of gene regulation, however, the replicates for the other two vehicles, especially GDI_3 exhibit more differentiated gene expression, which may be in part due to the small overall differences in gene expression between samples. Importantly, however, clustering confirmed that both MPO and NOX1 genes are co-regulated, in addition to several anti-oxidant (Gstp1, SOD2) and pro-inflammatory genes (Tnf, Il1b, Bcl6) that also appear co-regulated in these samples (Fig. 6).

While the PCR-array analysis provides a robust and a relatively high throughput method for assessing the transcript regulation of multiple target genes at once, it is also quite sensitive to the timing of exposure, since, as noted earlier, gene expression changes on mRNA level can occur quite rapidly (Li et al., 2015). In addition, even a substantial increase at the mRNA level of a gene does not guarantee that an upregulation of a gene ***protein*** will also be observed, e.g. due to potential post-transcriptional regulatory steps. Therefore, it is useful to couple the PCR screening approach of identifying larger regulatory patterns (e.g., cluster analysis as presented above) with targeted protein measurements. To that end we employed ELISA technology, though its limitations include relatively low sensitivity (high detection limit), which can often be prohibitively poor for protein targets with a low expression level. This problem was exacerbated by the low masses available from the chassis dynamometer trials.

Based on the PCR results and taking under consideration the character of protein targets, two of the genes discussed above were quantified via ELISA: the pro-inflammatory cytokine TNFα (Fig. 7a) and a cytoprotective, anti-inflammatory and an antioxidant-response gene HMOX-1 (Fig. 7b). Their expression was assessed in the NR8383 alveolar macrophages exposed for 6 h to PM extracts from three of the four GDIs (GDI_2 samples had insufficient mass). The results presented (Fig. 7a and b) are corrected for the basal expression of these proteins measured in a corresponding untreated (buffer only) control. Since the low-emitting vehicle was excluded, the overall range for both the TNFα and HMOX-1 protein data was much smaller and more comparable across the vehicles than the ROS and DTT ranges that included the GDI_2. The TNFα protein level expressed as an emission factor (i.e., per mile) varied <3-fold across all samples (Fig. 7a) and the per car average results varied <2-fold. The 3-car average PM mass-normalized induction of TNFα protein secretion (274 pg/mg PM) is low in comparison to ambient PM studies that ranged from 100 to 300,000 pg/mg PM (Shafer et al., 2016; Heo et al., 2015).

The data range of HMOX-1 expression measured in our study was very similar to TNFα, with the exception of the per-car averages, where the range was slightly larger (due primarily to the negative, though not significantly different than zero, values resulting from a higher expression level of HMOX-1 in the untreated control (Fig. 7b). Relative to control, GDI_4 induced the lowest levels of HMOX-1 (−15 ng/mi), followed by GDI_3 (73 ng/mi) and GDI_1 (214 ng/mi). It is difficult to directly compare the protein levels of HMOX-1 expressed in this study to these induced by other aerosol materials due to the paucity of published information. However, several studies of diesel particulates, black carbon and crystalline silica reported an increase in

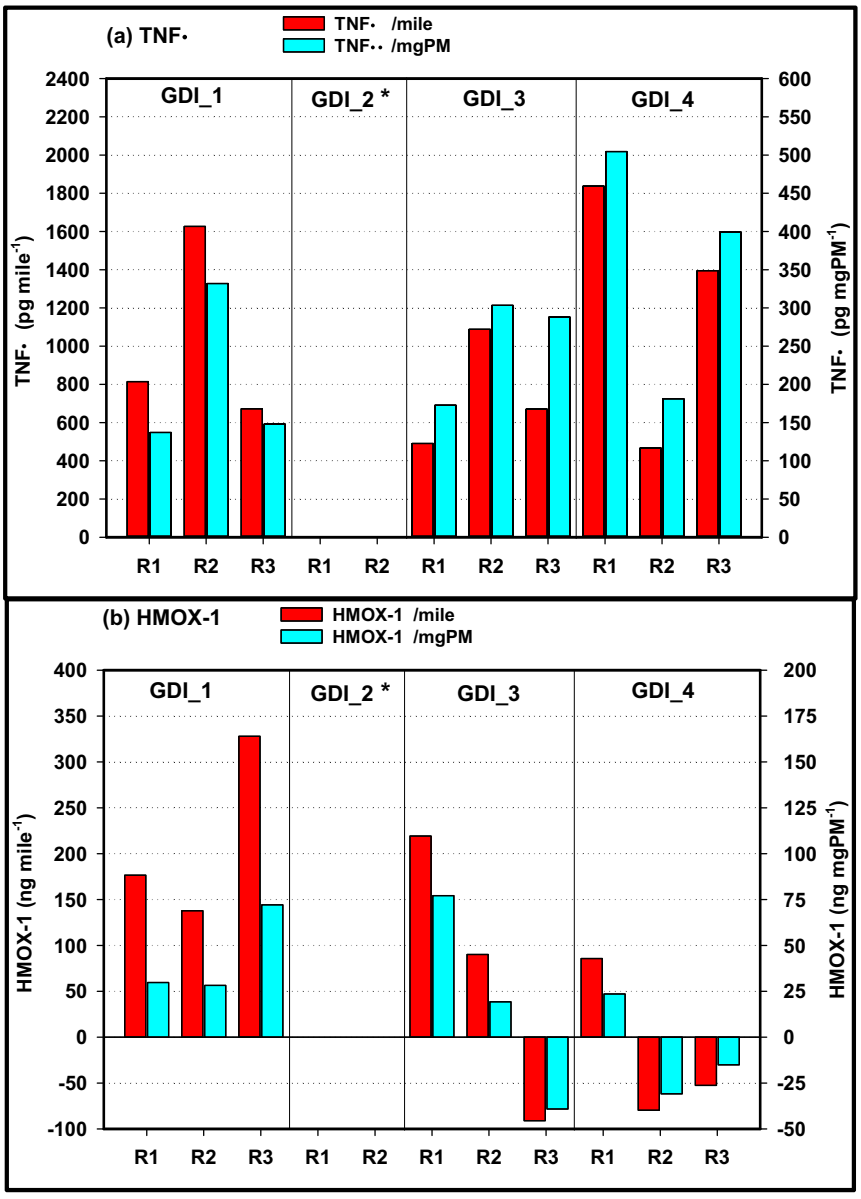

Fig. 7. Protein expression response (ELISA) corrected for the baseline expression of untreated control cells for tumor necrosis factor alpha (TNFα, a) and heme oxygenase 1 (HMOX-1, b) following 6 h exposure to vehicular exhaust extracts. Note that the asterisk (*) in the plot indicates that the assay was not performed due to insufficient PM mass.

expression of HMOX-1 in various exposure systems (Van Berlo et al., 2010; Koike and Kobayashi, 2006; Fukui et al., 2016). In contrast, multiple studies have reported the effects of aerosols on both inflammatory cytokines and antioxidant response genes at the mRNA level (PCR analysis). Interestingly, a differential expression profile of pro-inflammatory TNFα and the oxidative stress-related HMOX-1 has been reported for both ambient PM, as well as gasoline vehicular exhaust and diesel exhaust particles (DEP) suggesting that the expression of ***oxidative stress markers*** is potentially driven by different components of PM than the ***pro-inflammatory markers*** (Heo et al., 2015; Hamad et al., 2016; Bisig et al., 2015; Totlandsdal et al., 2015).

Two redox active metals (Fe and Ni) were moderately correlated with TNFα expression (Table 1). Two rare earth (REE) elements (Ce with TNFα; and Y with HMOX-1) exhibit correlations with the measured proteins. Molybdenum was correlated with HMOX-1 expression, and as noted in the water extractable metals discussion, was present in the PM at relatively high concentrations. As noted previously, the REE findings are consistent with those found with the oxidative activity metrics (ROS and DTT) and likely suggest a role for small insoluble particles in inducing oxidative stress, either directly or by providing a catalytic particle surface.

4. Conclusions

This work examined the physical and toxicological properties of particulate emissions from current technology GDI light-duty vehicles while operating over the LA92 driving cycle. Our results showed that three of the four GDI vehicles tested had PM emissions from 3 to 5 mg/mile, while one emitted about 0.2 mg/mile, thus showing the technical possibility for significant reductions. From an environmental standpoint, GDI vehicles are still an important source of ultrafine particles, especially in densely populated areas. Our findings showed that PM mass, particle number, and black carbon emissions during the cold-start phase of the LA92 cycle were higher than in the hot running or hot-start phases. In the case of the cleanest vehicle, the difference between cold-start and hot-start emissions was >10-fold. Under both hot and cold

conditions, PM emission rates were highest at engine start and during the hard accelerations in the test cycle.

The toxicology metrics employed in this study indicate that at least for acute exposure, toxicity is relatively low in comparison to many ambient PM samples, both for ROS generation and for inflammatory potential. DTT and ROS follow a different activity profile across the samples which is likely due to contrasts in PM composition, but additional studies with larger statistical power will be needed to better resolve those relationships. Our transcript analysis suggests that by 4 h of exposure protective mechanisms are at work trying to restore homeostasis: HMOX-1 is cyto-protective, an anti-oxidant response battery gene, and also upregulates IL-10 (an anti-inflammatory cytokine, which we saw in one sample). The overall suite of toxicology measurements suggests a likely role for small insoluble particles in inducing oxidative stress, either directly or by providing a catalytic particle surface. Ultrafine particles can partition into the blood stream from the lungs and can travel to other organs including the brain – whole animal studies will be needed to address these systemic effects; effects on macrophages can be especially important since the microglia in the brain share some responses are key players in some neurodegenerative diseases.

Acknowledgements

We acknowledge funding from the South Coast Air Quality Management District (SCAQMD) under contract 15625. The authors thank Mr. Mark Villela and Daniel Gomez of the University of California, Riverside for their contribution in conducting the emissions testing for this program. We also wish to acknowledge Dr. Jocelyn Hemming of the UW-WSLH Environmental Toxicology Program for conducting the DTT analyses and assisting with the macrophage ROS and other assays; and Joel Overdier of the UW-WSLH Trace Element Research Group for performing the SF-ICPMS measurements.

Appendix A. Supplementary data

Supplementary data to this article can be found online at https://doi.org/10.1016/j.scitotenv.2018.09.110.

References

Araujo, J.A., Nel, A.E., 2009. Particulate matter and atherosclerosis: role of particle size, composition and oxidative stress. Part Fibre Toxicol 24.
Attar, M.A., Xu, H., 2016. Correlations between particulate matter emissions and gasoline direct injection spray characteristics. J. Aerosol Sci. 102, 128–141.
Badshah, H., Kittelson, D., Northrop, W., 2016. Particle Emissions From Light-Duty Vehicles During Cold-Cold Start. SAE Technical Paper (2016-01-0997).
Bahreini, R., Xue, J., Johnson, K., Durbin, T., Quiros, D., Hu, S., Huai, T., Ayala, A., Jung, H., 2015. Characterizing emissions and optical properties of particulate matter from PFI and GDI light-duty gasoline vehicles. J. Aerosol Sci. 90, 144–153.
Barrientos, E.J., Anderson, J.E., Maricq, M.M., Boehman, A.L., 2016. Particulate matter indices using smoke point for vehicle emissions with gasoline, ethanol blends, and butanol blends. Combust. Flame 167, 308–319.
Bates, J.T., Weber, R.J., Abrams, J., Verma, V., Fang, T., Klein, M., Tolbert, P.E., 2015. Reactive oxygen species generation linked to sources of atmospheric particulate matter and cardiorespiratory effects. Environ. Sci. Technol. 49, 13605–13612.
Bisig, C., Steiner, S., Comte, P., Czerwinski, J., Mayer, A., Petri-Fink, A., Rothen-Rutishauser, B., 2015. Biological effects in lung cells in vitro of exhaust aerosols from a gasoline passenger car with and without particle filter. Emission Control Sci. Technol. 1, 237–246.
Bisig, C., Comte, P., Gudel, M., Czerwinski, J., Mayer, A., Muller, L., Petri-Fink, A., Rothen-Rutishauser, B., 2018. Assessment of lung cell toxicity of various gasoline engine exhaust using a versalite in vitro exposure system. Environ. Pollut. 235, 263–271.
Chan, T.W., Meloche, E., Kubsh, J., Brezny, R., 2014. Black carbon emissions in gasoline exhaust and a reduction alternative with a gasoline particulate filter. Environ. Sci. Technol. 48, 6027–6034.
Charrier, J.G., Anastasio, C., 2012. On dithiothreitol (DTT) as a measure of oxidative potential for ambient particles: evidence for the importance of soluble transition metals. Atmos. Chem. Phys. 12, 9321–9333.
Chen, L., Stone, R., Richardson, D., 2012. A study of mixture preparation and PM emissions using a direct injection engine fueled with stoichiometric gasoline/ethanol blends. Fuel 96, 120–130.
Cheng, Y., Wang, J., Zhuang, R., Wu, N., 2001. Analysis of combustion behavior during cold-start and warm-up process of SI gasoline engine. SAE Technical Paper (2001-01-3557).
Daher, N., Saliba, N.A., Shihadeh, A.L., Jaafar, M., Baalbaki, R., Shafer, M.M., Schauer, J.J., Sioutas, C., 2014. Oxidative potential and chemical speciation of size-resolved particulate matter (PM) at nearfreeway and urban background sites in the greater Beirut area. Science of the Total Environment 470–471, 417–426.
Diaz, E.A., Chung, Y., Papapostolou, V., Lawrence, J., Long, M.S., Hatakeyama, V., Gomes, B., Calil, Y., Sato, R., Koutrakis, P., Godleski, J.J., 2012. Effects of fresh and aged vehicular exhaust emissions on breathing pattern and cellular responses-pilot single vehicle study. Inhal. Toxicol. 25, 288–295.
Freire, J., Ajona, D., De Biurrun, G., Agorreta, J., Segura, V., Guruceaga, E., Bleau, A.M., Pio, R., Blanco, D., Montuega, L.M., 2013. Silica-induced chronic inflammation promotes lung carcinogenesis in the context of an immunosuppressive microenvironment. Neoplasia 15, 913–924.
Fukui, H., Endoh, S., Shichiri, M., Ishida, N., Hagihara, Y., Yoshida, Y., Iwahashi, H., Horie, M., 2016. The induction of lipid peroxidation during the acute oxidative stress response induced by intratracheal instillation of fine crystalline silica particles in rats. Toxicol. Ind. Health 32, 1430–1437.
Ghio, A.J., Carraway, M.S., Madden, M.C., 2012. Composition of air pollution particles and oxidative stress in cells, tissues, and living systems. J. Toxicol. Environ. Health B Crit. Rev. 1, 1–21.
Hamad, S.H., Schauer, J.J., Antkiewicz, D.S., Shafer, M.M., Kadhim, AKh, 2016. ROS production and gene expression in alveolar macrophages exposed to PM(2.5) from Baghdad, Iraq: seasonal trends and impact of chemical composition. Sci. Total Environ. 543, 739–745.
He, X., Ratcliff, M.A., Zigler, B.T., 2010. Effects of gasoline direct injection engine operating parameters on particle number emissions. Energy Fuel 26, 2014–2027.
Heo, J., Antkiewicz, D.S., Shafer, M.M., Perkins, D.A.K., Sioutas, C., Schauer, J.J., 2015. Assessing the role of chemical components in cellular responses to atmospheric particle matter (PM) through chemical fractionation of PM extracts. Anal. Bioanal. Chem. 405, 5953–5963.
Herner, J.D., Hu, S., Robertson, W.H., Huai, T., Oliver Chang, M.C., Rieger, P., Ayala, A., 2011. Effect of advanced aftertreatment for PM and NOx reduction on heavy-duty diesel engine ultrafine particle emissions. Environ. Sci. Technol. 45, 2413–2419.
Hideki, S., 2008. Structure, regulation and evolution of Nox-family NADPH oxidases that produce reactive oxygen species. FEBS J. 275, 3249–3277.
Hyde, T.L., Sankar, G., 2014. Solid state platinum speciation from X-ray absorption spectroscopic studies of fresh and road aged three way and diesel vehicle emission control catalysts. Platinum Metals in the Environment, Environmental Science and Engineering (ESE) Book Series. Springer, pp. 289–308.
Jomova, K., Baros, S., Valko, M., 2012. Redox active metal-induced oxidative stress in biological systems. Transit. Met. Chem. 37, 127–134.
Karavalakis, G., Short, D., Vu, D., Villela, M., Asa-Awuku, A., Durbin, T.D., 2014. Evaluating the regulated emissions, air toxics, ultrafine particles, and black carbon from SI-PFI and SI-DI vehicles operating on different ethanol and iso-butanol blends. Fuel 128, 410–421.
Karavalakis, G., Short, D., Vu, D., Russell, R., Hajbabaei, M., Asa-Awuku, A., Durbin, T.D., 2015a. Evaluating the effects of aromatics content in gasoline on gaseous and particulate matter emissions from SI-PFI and SI-DI vehicles. Environ. Sci. Technol. 49, 7021–7031.
Karavalakis, G., Short, D., Vu, D., Russell, R.L., Asa-Awuku, A., Jung, H., Johnson, K.C., Durbin, T.D., 2015b. The impact of ethanol and iso-butanol blends on gaseous and particulate emissions from two passenger cars equipped with spray-guided and wall-guided direct injection SI (spark ignition) engines. Energy 82, 168–179.
Karavalakis, K., Gysel, N., Schmitz, D.A., Cho, A.K., Sioutas, C., Schauer, J.J., Cocker, D.R., Durbin, T.D., 2017. Impact of biodiesel on regulated and unregulated emissions, and redox and proinflammatory properties of PM emitted from heavy-duty vehicles. Sci. Total Environ. 584–585, 1230–1238.
Koczak, J., Boehman, A., Brusstar, M., 2016. Particulate emissions in GDI vehicle transients: An examination of FTP, HWFET, and US06 measurements. SAE Technical Paper (2016-01-0992).
Koike, E., Kobayashi, T., 2006. Chemical and biological oxidative effects of carbon black nanoparticles. Chemosphere 65, 946–951.
Li, Y., Varala, K., Coruzzi, G.M., 2015. From milliseconds to lifetimes: tracking the dynamic behavior of transcription factors in gene networks. Trends Genet. 31, 509–515.
Lund, A.K., Knuckles, T.L., Akata, C.O., Shohet, R., McDonald, J.D., Gigliotti, A., Seagrave, J.C., Campen, M.J., 2007. Gasoline exhaust emissions induce vascular remodeling pathways involved in atherosclerosis. Toxicol. Sci. 95, 485–494.
Maikawa, C.L., Zimmerman, N., Rais, K., Shah, M., Hawley, B., Pant, P., Jeong, C.H., Delgado-Saborit, J.M., Volkens, J., Evans, G., Wallace, J.S., Godri Pollitt, K.J., 2016. Murine precision-cut lung slices exhibit acute responses following exposure to gasoline direct injection engine emissions. Sci. Total Environ. 568, 1102–1109.
Moldovan, M., 2007. Origin and fate of platinum group elements in the environment. Anal. Bioanal. Chem. 388, 537–540.
Odobasic, D., Kitching, A.R., Holdsworth, S.R., 2016. Neutrophil-mediated regulation of innate and adaptive immunity: the role of myeloperoxidase. J. Immunol. Res. https://doi.org/10.1155/2016/2349817 (Article ID 2349817, 11 pages).
Peckham, M., Finch, A., Campell, B., Price, P., Davies, M.T., 2011. Study of particle number emissions from a turbocharged gasoline direct injection (GDI) engine including data from a fast-response particle size spectrometer. SAE Technical Paper (2011-01-1224).
Piock, W., Hoffmann, G., Berndorfer, A., Salemi, P., Fusshoeller, B., 2011. Strategies towards meeting future particulate matter emission requirements in homogeneous gasoline direct injection engines. SAE Int. J. Engines 4, 1455–1468.
Pirjola, L., Karjalainen, P., Heikkila, J., Saari, S., Tzamkiozis, T., Ntziachristos, L., Kulmala, K., Keskinen, J., Ronkko, T., 2015. Effects of fresh lubricant oils on particle emissions emitted by a modern gasoline direct injection passenger car. Environ. Sci. Technol. 49, 3644–3652.

Quiros, D.C., Zhang, S., Sardar, S., Kamboures, M.A., Eiges, D., Zhang, M., Jung, H.S., Mcarthy, M.J., Chang, M.C.O., Ayala, A., Zhu, Y., Huai, T., Hu, S., 2015. Measuring particulate emissions of light duty passenger vehicles using integrated particle size distribution (IPSD). Environ. Sci. Technol. 49, 5618–5627.
Reed, M.D., Barret, E.G., Campen, M.J., Divine, K.K., Gigliotti, A.P., McDonald, J.D., Seagrave, J.C., Mauderly, J.L., Seilkop, S.K., Swenberg, J.A., 2008. Health effects of subchronic inhalation exposure to gasoline engine exhaust. Inhal. Toxicol. 20, 1125–1143.
Rohr, A.C., Wyzga, R.E., 2012. Attributing health effects to individual particulate matter constituents. Atmos. Environ. 62, 130–152.
Saffari, A., Daher, N., Shafer, M.M., Schauer, J.J., Sioutas, C., 2014a. Global perspective on the oxidative potential of airborne particulate matter: a synthesis of research findings. Environ. Sci. Technol. 48, 7576–7583.
Saffari, A., Daher, N., Shafer, M.M., Schauer, J.J., Sioutas, C., 2014b. Seasonal and spatial variation in dithiothreitol (DTT) activity of quasi-ultrafine particles (PM0.25) in the Los Angeles Basin and its association with chemical species. J. Environ. Sci. Health A 49, 441–451.
Saffari, A., Hasheminassab, S., Shafer, M.M., Schauer, J.J., Chatila, T.A., Sioutas, C., 2016. Nighttime aqueous-phase secondary organic aerosols in Los Angeles and its implication for fine particulate matter composition and oxidative potential. Atmos. Environ. 113, 112–122.
Sakai, S., Hageman, M., Rothamer, D., 2013. Effect of equivalence ratio on the particulate emissions from a spark-ignited, direct-injected gasoline engine. SAE Technical Paper (2013-01-1560).
Seagrave, J.C., McDonald, J.D., Gigliotti, A.P., Nikula, K.J., Seilkop, S.K., Curevich, M., Mauderly, J.L., 2002. Mutagenicity and in vivo toxicity of combined particulate and semivolatile organic fractions of gasoline and diesel engine emissions. Toxicol. Sci. 70, 212–226.
Shafer, M.M., Hemming, J.D.C., Antkiewicz, D.S., Schauer, J.J., 2016. Oxidative potential of size-fractionated atmospheric aerosol in urban and rural sites across Europe. Faraday Discuss. 189, 381.
Siddiqui, M.A., Saquib, Q., Ahamed, M., Farshori, N.N., Ahmad, J., Wahab, R., Khan, S.T., Alhadlaq, H.A., Musarrat, J., Al-Khedhairy, A.A., 2015. Molybdenum nanoparticles-induced cytotoxicity, oxidative stress, G2/M arrest, and DNA damage in mouse skin fibroblast cells (L929). Colloids Surf. B: Biointerfaces 125, 73–81.
Sijan, Z., Antkiewicz, D.S., Heo, J., Kado, N.Y., Schauer, J.J., Sioutas, C., Shafer, M.M., 2015. An in vitro alveolar macrophage assay for the assessment of inflammatory cytokine expression induced by atmospheric particulate matter. Environ. Toxicol. 30, 836–851.
Sobotowski, R.A., Butler, A.D., Guerra, Z., 2015. A pilot study of fuel impacts on PM emissions from light-duty gasoline vehicles. SAE Technical Paper (2015-01-9071).
Sonntag, D.B., Baldauf, R.W., Yanca, C.A., Fulper, C.R., 2014. Particulate matter speciation profiles for light-duty gasoline vehicles in the United States. J. Air Manag. Assoc. 64, 529–545.
Su, J., Lin, W., Sterniak, J., Xu, M., Bohac, S.V., 2014. Particulate matter emission comparison of spark ignition direct injection (SIDI) and port fuel injection (PFI) operation of a boosted gasoline engine. J. Eng. Gas Turbines Power 136 (091513-1-091513-6).
Szybist, J.P., Youngquist, A.D., Barone, T.L., Storey, J.M., Moore, W.R., Foster, M., Confer, K., 2011. Ethanol blends and engine operating strategy effects on light-duty spark ignition engine particle emissions. Energy Fuel 25, 4977–4985.
Tamagawa, E., Bai, N., Morimota, K., Gray, C., Mui, T., Yatera, K., Zhang, X., Xing, L., Li, Y., Laher, I., Sin, D.D., Man, S.F.P., van Eeden, S.F., 2008. Particulate matter exposure induces persistent lung inflammation and endothelial dysfunction. Am. J. Physiol. Lung Cell. Mol. Physiol. 295, L79–L85.
Tan, C., Xu, H., Ma, H., Ghafourian, A., 2014. Investigation of VVT and spark timing on combustion and particle emission from a GDI engine during transient operation. SAE Technical Paper (2014-01-1370).
Totlandsdal, A.I., Låg, M., Lilleaas, E., Cassee, F., Schwarze, P., 2015. Differential proinflammatory responses induced by diesel exhaust particles with contrasting PAH and metal content. Environ. Toxicol. 30, 188–196.
Tzamkiozis, T., Stoeger, T., Cheung, K., Ntziachristos, L., Sioutas, C., Samaras, Z., 2010. Monitoring the inflammatory potential of exhaust particles from passenger cars in mice. Inhal. Toxicol. 22, 59–69.
Uy, D., Ford, M.A., Jayne, D.T., O'Neil, A.E., Haack, L.P., Hangas, J., Jagner, M.J., Sammut, A., Gangopadhyay, A.K., 2014. Characterization of Gasoline Soot and Comparison to Diesel Soot: Morphology, Chemistry, and Wear. 80 pp. 198–209.
Van Berlo, D., Albrecht, C., Knaapen, A.M., Cassee, F.R., Gerlofs, M.E., Kooter, I.M., Palomero-Gallagher, N., Bidmon, H.J., van Schooten, F.J., Krutmann, J., Schins, R.P.F., 2010. Comparative evaluation of the effects of short-term inhalation exposure to diesel engine exhaust on rat lung and brain. Arch. Toxicol. 84, 553–562.
Verma, V., Ning, Z., Cho, A.K., Schauer, J.J., Shafer, M.M., Sioutas, C., 2009. Redox activity of urban quashi-ultrafine particles from primary and secondary sources. Atmos. Environ. 43, 6360–6368.
Verma, V., Shafer, M.M., Schauer, J.J., Sioutas, C., 2010. Contribution of transition metals in the reative oxygen species activity of PM emissions from retrofitted heavy-duty vehicles. Atmos. Environ. 44, 5165–5173.
Wang, X., Grose, M.A., Caldow, R., Osmondson, B.L., Swanson, J.J., Chow, J.C., Watson, J.G., Kittelson, D.B., Li, Y., Xue, J., Jung, H., Hu, S., 2016. Improvement of engine exhaust particle sizer (EEPS) size distribution measurement – II. Engine exhaust particles. J. Aerosol Sci. 92, 83–94.
Xu, F., Chen, L., Stone, R., 2011. Effects of a catalytic volatile particle remover (VPR) on the particulate matter emissions from a direct injection spark ignition engine. Environ. Sci. Technol. 45, 9036–9043.
Xue, J., Quiros, D., Wang, X., Durbin, T.D., Johnson, K.C., Karavalakis, G., Hu, S., Huai, T., Ayala, A., Jung, H.S., 2016. Using a new inversion matrix for a fast-sizing spectrometer and a photo-acoustic instrument to determine suspended particulate mass over a transient cycle for light-duty vehicles. Aerosol Sci. Technol. 50, 1227–1238.
Zhang, S., McMahon, W., 2012. Particulate emissions for LEV II light-duty gasoline direct injection vehicles. SAE Int. J. Fuels Lubr. 5, 637–646.
Zinola, S., Raux, S., Leblanc, M., 2016. Persistent particle number emissions sources at the tailpipe of combustion engines. SAE Technical Paper (2016-01-2283).